High-speed underwater wireless optical communications: from a perspective of advanced modulation formats [Invited]

Chao Fei (费 超)[1,2,†], Xiaojian Hong (洪晓建)[1,2,†], Ji Du (杜 及)[1,2], Guowu Zhang (张国务)[1,2], Yuan Wang (王 远)[1,2], Xiaoman Shen (申晓曼)[1,2], Yuefeng Lu (陆岳锋)[1,2], Yang Guo (郭 旸)[1,2], and Sailing He (何赛灵)[1,2,*]

[1]*Centre for Optical and Electromagnetic Research, National Engineering Research Center for Optical Instruments, Zhejiang University, Hangzhou 310058, China*

[2]*Ningbo Research Institute, Zhejiang University, Ningbo 315100, China*

**Corresponding author: sailing@kth.se*

Received August 30, 2019; accepted September 12, 2019; posted online October 14, 2019

In this paper, recent advances in underwater wireless optical communication (UWOC) are reviewed for both LED- and LD-based systems, mainly from a perspective of advanced modulation formats. Volterra series-based nonlinear equalizers, which can effectively counteract the nonlinear impairments induced by the UWOC system components, are discussed and experimentally demonstrated. Both the effectiveness and robustness of the proposed Volterra nonlinear equalizer in UWOC systems under different water turbidities are validated. To further approach the Shannon capacity limit of the UWOC system, the probabilistic constellation shaping technique is introduced, which can overcome the inherent gap between a conventional regular quadrature amplitude modulation (QAM) format and the Shannon capacity of the channel. The experimental results have shown a significant system capacity improvement compared to the cases using a regular QAM.

OCIS codes: 060.2605, 060.4080, 140.7300, 010.4450.
doi: 10.3788/COL201917.100012.

As increase in the ongoing expansion of human activities in ocean environments, such as oceanographic research, offshore oil exploration, tactical surveillance, pollution monitoring, and underwater salvage, high-bandwidth data transfer, like the exchange of large volumes of data files between fixed sensor nodes and autonomous underwater vehicles (AUVs) or remotely operated vehicles (ROVs), shuttling real-time video from untethered vehicles for inspection and identification, is indispensable. The mature technology of acoustic communication could support transmission distances of tens of kilometers[1], but its drawbacks include low bandwidth, low data rate (~kbps), severe multipath latency, high energy consumption, and lack of stealthiness[2]. Radio frequency (RF) communication, while effective in terrestrial applications, is severely restricted in the ocean due to the exponential decay at radio frequencies in seawater, e.g., the attenuation in the ocean is about 169 dB/m for the 2.4 GHz band[3]. Thus, RF communication can only work at ultralow frequencies, supporting near-field communication, and consequently paradoxically limits its bandwidth. Moreover, RF-based communication requires huge antennas and high power, which poses more challenges to cost and energy efficient oceanic applications. Tethered fiber-optic cables can offer robust and high-bandwidth communication, but they face sophisticated engineering and maintenance issues and are not appropriate for underwater moving platforms[4]. Moreover, the deep ocean environment is challenging, which makes optical connectors very expensive and short-lived. Underwater wireless optical communication (UWOC) turns out to be an appropriate solution for communication over short and medium ranges (within hundreds of meters) due to its high bandwidth, low latency, cost-effectiveness, and low energy consumption.

In recent years, UWOC has attracted considerable interest from academic, industrial, and military circles, and is deemed as a revolutionary and competitive technology to its acoustic and RF counterparts, particularly when applied in broadband communications between diverse underwater vehicles, underwater sensor nodes, and underwater base stations[5]. Blue-green wavelengths of the visible light spectrum are found to be in the low absorption window of seawater[6,7]. Light-emitting diodes (LEDs) or laser diodes (LDs) are widely employed as transmitters of UWOC systems. An LED features low-cost and high-energy efficiency, and the broad-angle beam profile of an LED can relax the alignment requirement of the transmitter and receiver. However, the broad-angle beam profile makes an LED more susceptible to scattering in natural waters. The emitted optical power from an LED can only support a relatively short transmission distance. The product BlueComm 200 from Sonardyne[8] can sustain a maximum distance of 150 m using a highly sensitive receiver photomultiplier tube (PMT). Furthermore, the bandwidths of LEDs are limited to the order of MHz (e.g., the 3 dB bandwidth of LED was ~20 MHz in Ref. [9], 160 MHz in Ref. [10], and 752 MHz in Ref. [11]). On the contrary, the bandwidths of LDs are much larger (e.g., the 3 dB bandwidth of an LD was ~1.4 GHz in Ref. [12], 2.6 GHz in Ref. [13], and 5.3 GHz in Ref. [14]). Meanwhile, LDs can be collimated into very narrow beam profiles that

will significantly increase the optical power delivered to a remote undersea terminal. Meanwhile, an extremely narrow laser beam can reduce the temporal spread of the signal and enable enhanced spatial and spectral filtering options to reduce the background light noise[15]. The significant hurdle for a reliable LD-based UWOC is the link alignment, which may require the pointing, acquisition, and tracking (PAT) system.

With the increased attention in UWOC research, several surveys have been published to review this emerging subject. In Ref. [16], Arnon evaluated the link performance of a typical UWOC system and analyzed several UWOC link models, including the line-of-sight (LOS) link, the modulating retroreflector link, and the reflective link. Hemani *et al.* discussed various propagation phenomena that impacted the performance of a UWOC system and reviewed recent research progress in UWOC, including channel characterization, modulation schemes, coding techniques, and various sources of noise that are specific to UWOC[17]. In Ref. [18], Zeng *et al.* provided an exhaustive survey of the state-of-the-art UWOC research in three aspects: channel characterization, modulation, and coding techniques, together with the practical implementations of UWOC. Nasir *et al.* presented a comprehensive survey on the challenges, advances, and prospects of underwater optical wireless networks from a layer by layer perspective, and pointed out the prospective directions for UWOC, networking, and localization studies[19]. In Ref. [20], the authors provided a detailed comparison of applying three advanced modulation formats, including carrierless amplitude and phase (CAP) modulation, orthogonal frequency division multiplexing (OFDM), and discrete Fourier transform spread orthogonal frequency division multiplexing (DFT-S OFDM) in LED-based UWOC systems. In Ref. [21], the authors gave a review on the recent advances and highlights in LD-based UWOC systems from a device perspective, mainly focused on LDs. In the present paper, we review recent research progress in the UWOC subject, mainly from a perspective of advanced modulation formats, focusing on both LED- and LD-based UWOC systems. In addition, some studies of channel modeling used for simulation and other characteristics (such as the turbulence) that may remarkably affect the UWOC performance are mentioned briefly.

It is important to understand aquatic optical channel characterization before conducting a UWOC experiment. Monte Carlo simulation is a popular numerical method achieved by sending and tracking the trajectories of a large number of emitted photons[22,23]. In Ref. [24], the authors designed a Monte Carlo simulator and the simulation results showed that the UWOC distance could be extended to 500 m in pure seawater when a single photon avalanche diode (SPAD) was employed as the receiver. Gabriel *et al.* used the two-term Henyey–Greenstein (HG) channel model to quantify the time dispersion of the UWOC channel for different water types, link distances, and transmitter/receiver characteristics. The performance of a typical UWOC system in terms of bit error rate (BER) using on–off keying (OOK) modulation was studied[25]. By taking into account three types of propagating photons including non-scattering, single, and multiple scattering, the authors presented a general stochastic channel model that fits well with Monte Carlo simulations in coastal and turbid water channels[26]. In Ref. [27], Tang *et al.* proposed a closed-form double-gamma function to model the channel impulse response of a UWOC system. This impulse response is able to evaluate the BER and channel bandwidth for various link ranges of a UWOC system. Zhang *et al.* introduced a weighted gamma function polynomial (WGFP) to model the impulse response of general $M \times N$ multiple-input multiple-output (MIMO) UWOC links. Numerical results of Monte Carlo simulations validated the proposed WGFP model in a turbid water environment[28].

For a UWOC lab experiment, one principal target is to improve the capacity and extend the transmission distance of a UWOC system. Since the first experimental demonstration of high speed UWOC on the order of Gb/s[29], a lot of works have explored higher data rate and longer transmission distance in LED- or LD-based UWOC systems. Xu *et al.* have demonstrated a blue LED-based UWOC system using 16-QAM-OFDM, achieving a net bit rate of 161.36 Mb/s at a BER of 2.5×10^{-3}[30]. Tian *et al.* have reported a data rate of 800 Mb/s over a 0.6 m UWOC system using a micro-LED[10]. Kong *et al.* have proposed a UWOC system using an arrayed transmitter/receiver and optical superimposition-based pulse amplitude modulation with 4 levels (PAM-4), which enhanced tolerance to the modulation nonlinearities of LEDs[31]. Wang *et al.* have realized an OFDM-based UWOC system using a multipixel photon counter (MPPC) as the receiver, which has a high sensitivity and supports a relatively long underwater transmission distance[32]. In Ref. [33], the authors have proposed a UWOC system utilizing QAM-OFDM and multi-PIN reception for maximum ratio combination (MRC) receiving, acquiring a data rate of 2.175 Gb/s. Chi *et al.* have demonstrated a novel Gaussian kernel-aided deep neural network (GK-DNN) equalizer that can effectively mitigate the high nonlinear distortion of PAM8 LED-based UWOC systems[34]. Oubei *et al.* have conducted a lab experiment obtaining 4.8 Gb/s over 5.4 m underwater laser transmission using 16-QAM-OFDM[35]. Chen *et al.* have demonstrated 26 m / 5.5 Gb/s air-water channel transmission employing 32-QAM-OFDM[36]. Injection locking has been utilized to enhance the frequency response of LDs, and the authors have experimentally demonstrated a 16 Gb/s over 10 m[37] and a 25 Gb/s over 5 m[14] UWOC systems. Huang *et al.* have reported 14.8 Gb/s over 1.7 m seawater transmission using 16-QAM-OFDM with a modulation bandwidth of 3.7 GHz[38]. Our previous works have probed post nonlinear equalization and adaptive bit-power loading discrete multitone (DMT)-based UWOC systems under different water turbidities[39], and demonstrated 16.6 Gb/s over 5 m and 6.6 Gb/s over 55 m transmission[40]. We have also introduced multiband DFT-S to reduce the peak-to-average-power ratio (PAPR) of a DMT-based UWOC transmitter and improved the

BER performance of a long reach UWOC system[41]. We have probed probabilistic constellation shaping (PCS) in a DMT-based UWOC system to approach the underwater channel capacity limit, and the net data rate has been pushed to 18.09 Gb/s over a 5 m water channel with a single LD[42]. Hu *et al.* have demonstrated a 120 m distance in Jerlov II water for Reed–Solomon (RS) (255,127) code with 256 pulse-position modulation (PPM) at a bandwidth of 13.7 MHz[43]. 100 m/500 Mb/s LD-based UWOC has been experimentally demonstrated using OOK modulation and nonlinear equalization[44]. Al-Halafi *et al.* have probed real-time video streaming underwater optical wireless transmission using software defined platforms[45,46].

In terms of practical implementations of UWOC, the Woods Hole Oceanographic Institution (WHOI) designed an optical modem system based on omnidirectional LED arrays and hemispherical PMT in 2006, and validated 5 Mb/s over 91 m underwater transmission[47]. In 2008, they conducted a sea trial and successfully realized 5 Mb/s over 200 m UWOC in 2000 m deep ocean[48]. In 2014, the WHOI completed bi-directional UWOC between a seafloor test node and the AUV sentry within 20–150 m range at data rates of 5–10 Mb/s[49]. Researchers from Massachusetts Institute of Technology (MIT) built a UWOC prototype called AquaOptical[50], and achieved a data rate of 1.2 Mb/s at distances up to 30 m in a pool test. Afterward, they updated it to AquaOptical II[51] and reported reliable communication of 2 Mb/s over 50 m in pool water. The Japan Agency for Marine-Earth Science and Technology (JAMSTEC) has developed a UWOC system of 20 Mb/s over a 120 m communication distance in 700 m deep ocean water[52]. Cossu *et al.* have designed a full-fledged 10 Base-T Ethernet UWOC system, which is developed in the framework of the European Project SUNRISE[53], supporting 10 Mb/s over a 7.5 m distance in a shallow harbor water transmission[54], and 10 Mb/s over 10 m in a highly turbid harbor water transmission[55]. Baiden *et al.* have tested an omni-directional UWOC system in lake water[56], and demonstrated 20 Mb/s over 11 m transmission[57]. Han *et al.* have proposed a transmitter with a 150° divergence angle and more than 90% uniformity of radiation intensity for a quasi-omni-directional UWOC by applying a freeform lens into an LED array, and achieved 19 Mb/s over 8 m water channel transmission[58]. In Ref. [59], the authors designed a real-time field programmable gate array (FPGA)-based LED-UWOC system and demonstrated 25 Mb/s over a 10 m underwater channel. Shan *et al.* have built an underwater laser communication device with high pulse energy and small volume[60]. In Refs. [61–66], orbital angular momentum multiplexing (OAM) has been explored in a UWOC application as an emerging technique. Xu *et al.* have put forth a novel concept on an underwater fiber–wireless (Fi–Wi) communication system with a fully passive wireless front end, which can save sophisticated, expensive, and short-lived optical connectors in deep oceans[67].

Sun *et al.* have demonstrated a non-LOS UWOC link using an ultraviolet (UV) 375 nm laser to circumvent the alignment requirement of an LOS underwater link[68], and experimentally demonstrated high-speed diffuse LOS optical wireless communication across a wavy water-air interface[69]. In Refs. [70,71], the authors have experimentally investigated the impact of turbulence on a UWOC link. Table 1 summarizes some recent works of UWOC in the literature.

A schematic diagram of the general UWOC experimental setup in a lab is shown in Fig. 1. After being amplified and superimposed with DC, the transmitted RF signal from an arbitrary waveform generator (AWG) drives an LED/LD. The collimated light beam carrying the electrical signal passes through a water channel, is then captured by an APD/PIN, and finally seized by a digital serial analyzer (DSA) for further processing. The DMT modulation is a promising modulation scheme in UWOC for its intrinsic advantages such as high spectral efficiency and simple equalization. Moreover, the structure of cyclic prefix (CP) is inherently tolerant to inter-symbol interference (ISI) caused by multipath scattering in highly turbid waters. Nevertheless, the main drawback of DMT modulation is the high PAPR, which may induce severe nonlinear impairments and inefficient power utilization if advanced modulation formats are further employed. The nonlinearity widely exists in UWOC systems, which is mainly introduced by the modulation nonlinearity of an LED[74] or LD[75,76], the nonlinear amplification of an electrical amplifier[77,78], and the square-law detection of a photodetector[79]. Nonlinearity is common in single carrier systems such as multilevel PAM[80] and CAP[81] and multicarrier systems such as DMT. The nonlinear distortions induced by the LED (or LD), electrical amplifier, and photodetector may give severe impairments in the received signals, resulting in a significant signal-to-noise ratio (SNR) degradation. The linear equalization techniques cannot effectively counteract such nonlinear effects. Volterra series-based nonlinear equalizers have been intensively studied in wireless[82], fiber-optic communication[83], and free-space visible light communication (VLC) systems[80,81,84–86]. Biswas *et al.* analyzed the semiconductor LD nonlinearity from the laser rate equations using an output-to-input approach[75]. Hence, the nonlinearity in both LED- and LD-based UWOC systems can be modeled by the Volterra series, which is expressed as

$$y(n) = \sum_{k_1=0}^{N_1-1} w_1(k_1)x(n-k_1) + \sum_{k_1=0}^{N_2-1}\sum_{k_2=0}^{N_2-1} w_2(k_1,k_2)x(n-k_1)x(n-k_2) + \sum_{k_1=0}^{N_3-1}\sum_{k_2=0}^{N_3-1}\sum_{k_3=0}^{N_3-1} w_3(k_1,k_2,k_3)x(n-k_1)x(n-k_2)x(n-k_3) + \cdots, \quad (1)$$

Table 1. Summary of Recent Works in UWOC

Authors	Transmitter type	Light output power	Photo-detector	Modulation formats	Data rate	Distance (m)	Distance-data rate product (Gbps · m)	Real time
Xu *et al.*[30]	Blue LED	N/A	PIN	16-QAM-OFDM	161 Mb/s	2	0.32	N
Tian *et al.*[10]	440 nm micro-LED	N/A	PIN/APD	OOK	800/200 Mb/s	0.6/5.4	1.08	N
Wang *et al.*[33]	521 nm LED	160 mW	2 PINs	64-QAM-DMT, MRC	2.175 Gb/s	1.2	2.61	N
Zhou *et al.*[72]	RGBYC LED		PIN	Bit-power loading DMT	15.17 Gb/s	1.2	18.2	N
Wang *et al.*[59]	448 nm LED	N/A	APD	OOK	25 Mb/s	10	0.25	Y
Wang *et al.*[32]	520 nm LD	15 mW	MPPC	32-QAM-OFDM	312.03 Mb/s	21	6.55	N
Oubei *et al.*[35]	450 nm LD	15 mW	APD	16-QAM-OFDM	4.8 Gb/s	5.4	25.92	N
Chen *et al.*[36]	520 nm LD	15 mW	APD	32-QAM-OFDM	5.5 Gb/s	5/21	115.5	N
Liu *et al.*[73]	520 nm LD	19.4 mW	PIN/APD	OOK	2.7 Gb/s	34.5	93.15	N
Fei *et al.*[39]	450 nm LD	20 mW	APD	Bit-power loading DMT, NE	7.3 Gb/s	15	109.95	N
Fei *et al.*[41]	450 nm LD	12.8 mW	APD	MB-DFT-S-DMT	5.6 Gb/s	55	308	N
Fei *et al.*[40]	450 nm LD	120 mW	PIN	Bit-power loading DMT, NE	16.6/6.6 Gb/s	5/55	462@35 m	N
Li *et al.*[37]	Two 488 nm LDs	20 mW	PIN	PAM4, injection locking	16 Gb/s	10	160	N
Li *et al.*[14]	Three 680 nm LDs	3 mW	PIN	Injection locking, OOK	25 Gb/s	10	250	N
Huang *et al.*[38]	450 nm LD	120 mW	PIN/APD	16-QAM-OFDM	14.8/10.8 Gb/s	1.7/10.2	25.16/110	N
Hong *et al.*[42]	450 nm LD	120 mW	PIN	PCS-DMT	18.09/12.6 Gb/s	5/35	441@35 m	N
Wang *et al.*[44]	520 nm LD	15 mW	APD	OOK, NE	500 Mb/s	100	50	N
Hu *et al.*[43]	532 nm LD	N/A	SPD	256-PPM & RS, LDPC	~MHz	120	N/A	N
JAMSTEC[52]	450 nm LD	>5 W	PMT	N/A	20 Mb/s	120	2.4	Y

Where $y(n)$ denotes the nth received signal sample, and $w_1(k_1)$ and $w_m(k_1, k_2, \ldots, k_m)(m \geq 2)$ are the linear coefficient and mth-order nonlinear coefficient, respectively. $N_t\,(t \geq 1)$ is the memory length. $x(n-k_i)$ is the $(n-k_i)$ th temporal sample of transmitted signal. The Volterra series-based equalizer can be adopted to eliminate the nonlinear noise in UWOC systems. In our previous works[33,34], we proposed simplified Volterra nonlinear equalizers that include only the 2nd-order and partial 3rd-order nonlinear terms. With the simplified Volterra nonlinear equalizers, the received SNR of the system can be significantly enhanced by 2–3 dB[39,40]. After the combination with the adaptive bit-power loading DMT, the average modulation order (bits per symbol) increases from 4.97 to 5.87. With a modulation

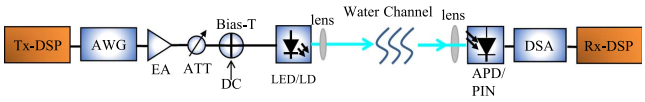

Fig. 1. Schematic diagram of the general UWOC setup in a lab experiment. AWG: arbitrary waveform generator; EA: electrical amplifier; ATT: adjustable attenuator; DC: direct current; LD: laser diode; APD: avalanche photodiode; DSA: digital serial analyzer; Tx-DSP: digital signal processing at the transmitter; Rx-DSP: digital signal processing at the receiver.

bandwidth of 1.25 GHz, the system capacities increase from 6.21 Gb/s to 7.33 Gb/s over a 15 m water channel[39]. In Ref. [40], with a modulation bandwidth of 2.75 GHz, the system capacities increase from 15.6 Gb/s to 16.6 Gb/s over a 5 m water channel. The nonlinear equalization can bring a capacity improvement of about 1 Gb/s in both cases. Figure 2 shows the received optical power (ROP, red line), SNR with nonlinear equalization (blue line), and SNR without nonlinear equalization (green line) versus transmission distance under tap water. The ROP decreases for longer transmission distances due to the absorption and scattering effects of water and the loss from multiple reflections by mirrors (used to simulate different water channel lengths). With the higher modulation depth allowed by the nonlinear equalization, the received SNR can be enhanced by ~3 dB compared to the linear equalization case.

The performance of our proposed scheme under different water turbidity conditions has been investigated. The received SNR under different water turbidities after a 1 m transmission distance is shown in Fig. 3(a). The water turbidity is changed by adding the 0.5% diluted Maalox [$Al(OH)_3$ and $Mg(OH)_2$ powder] suspension in 2 mL steps (a step of 20 mL after 30 mL) into the tap water (volume of ~85.7 L). The remarkable SNR gain of >3 dB, regardless of the water turbidity, shows the robustness of the nonlinear equalization method in UWOC systems. To quantify the turbidity of water, Fig. 3(b) shows the corresponding attenuation coefficient of water, which is calculated in Ref. [87]. The calculated

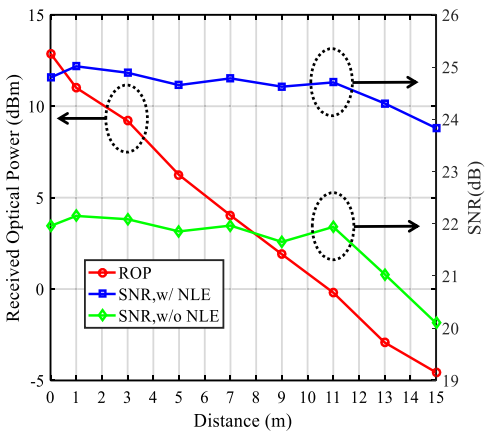

Fig. 2. Received optical power (ROP) and SNR versus transmission distance under tap water. w/: with; w/o: without; NLE: nonlinear equalization[39].

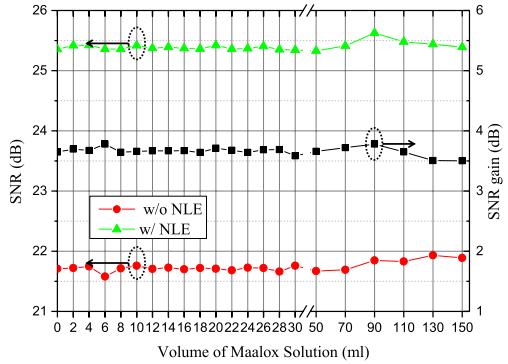

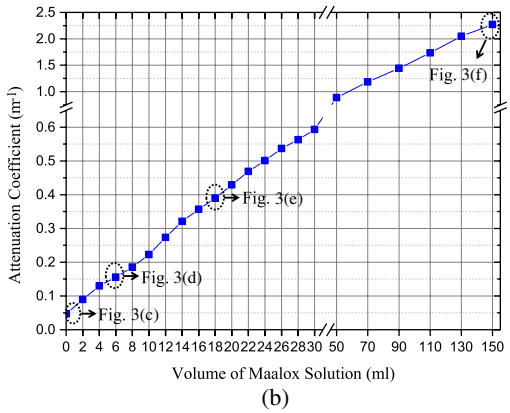

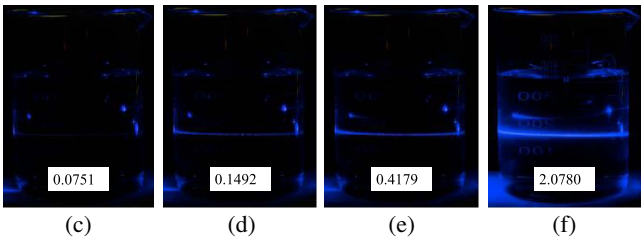

Fig. 3. (a) Received SNR versus the volume of added Maalox suspension after a 1 m underwater transmission. (b) Attenuation coefficient versus volume of the added Maalox suspension. (c)–(f) The snapshots of the optical beam passing through water of different turbidities which represent (c) "tap water", (d) "clear ocean", (e) "coastal ocean", and (f) "harbor water"[39].

attenuation coefficient ranges from 0.0751 m^{-1} to 2.078 m^{-1}, which covers the typical values of "clear ocean", "coastal ocean", and "harbor water"[29]. Figures 3(c)–3(f) present the side view of the optical beam passing through water with different turbidities. The snapshots were taken one by one under the same settings of exposure time and camera sensitivity. As can be seen from this figure, the scattered light becomes stronger with a larger dose of added Maalox suspension.

Apart from enhancing the SNR of the system, increasing system capacity is another hot topic in UWOC research. Recently, a powerful and flexible channel capacity limit-approaching technique, called PCS has been extensively studied in wireless communication[88] and fiber-optic communication[89,90], and introduced in the VLC area[91]. The PCS technique applied to high-order modulation formats has become an excellent candidate to

overcome the inherent gap between the conventional regular QAM format and the Shannon capacity of the channel. In our previous work[42], the PCS scheme with DMT modulation has been experimentally demonstrated in a UWOC system to approach the channel capacity limit. According to the pre-estimated SNR of each subcarrier, a fixed QAM format with various probabilistic distributions is individually allocated for each subcarrier to achieve maximum capacity. In DMT with the PCS scheme, different probability mass functions (PMFs) determined by a user-defined distribution matcher, e.g., the well-known Maxwell-Boltzmann distribution[88,90], are assigned to different subcarriers. Assuming that the PCS-MQAM constellation values are taken from $\chi = \{x_1, x_2, \ldots, x_M\}$, the corresponding PMF can be expressed as[88]

$$P(x_i) = e^{-\upsilon|x_i|^2} \Big/ \sum_{x\in\chi} e^{-\upsilon|x|^2}, \quad 1 \le i \le M, \tag{2}$$

where υ is a rate adjustable parameter. For a given target SNR range, there exists a suitable υ to optimize the constellation shaping, leading to an achievable maximum channel capacity. The optimization process can be performed via a look-up table.

The Shannon capacity limit $C = \log_2(1 + \mathrm{SNR})$[92] of different underwater transmission channels is presented in Fig. 4(a). From the figure, PCS-1024QAM is the optimal option for 5 m and 25 m underwater channels as the maximum Shannon capacity limit for the two cases is about 10 bits/symbol. Likewise, PCS-256QAM and PCS-64QAM are suitable for the 35 m and 45 m underwater channel cases, respectively. For the sake of simplicity, only the cases of 25 m with PCS-1024QAM-DMT and 35 m with PCS-256QAM-DMT underwater transmission channels are taken into discussion. For the bit-power loading scheme, different QAM formats are assigned to different subcarriers in accordance with the pre-estimated SNR, and the overall BER is below the 7% overhead standard hard-decision forward error correction (HD-FEC) limit of 3.8×10^{-3}. For the PCS scheme, a fixed QAM format with different probabilistic constellation distributions is employed based on the pre-estimated SNR. Figure 4(b) shows the entropy versus subcarrier index for the bit-power loading and PCS schemes. The entropy of bit-power loading can only take discrete integer bits while the PCS can take continuous values (less than $\log_2 M$ for PCS-MQAM scheme). The entropy of DMT with the PCS scheme of each subcarrier is larger than that with the bit-power loading scheme, implying that the PCS scheme can carry more information than the latter. Figure 4(c) exhibits the graphical illustrations of three regular QAM formats (i.e., 128QAM/64QAM/32QAM) for bit-power loading and three adopted constellation probability distributions for both PCS-256QAM-DMT (35 m channel) and PCS-1024QAM-DMT (25 m channel). The distributions become more centralized as entropy H decreases, and the occurrence probability of the outer

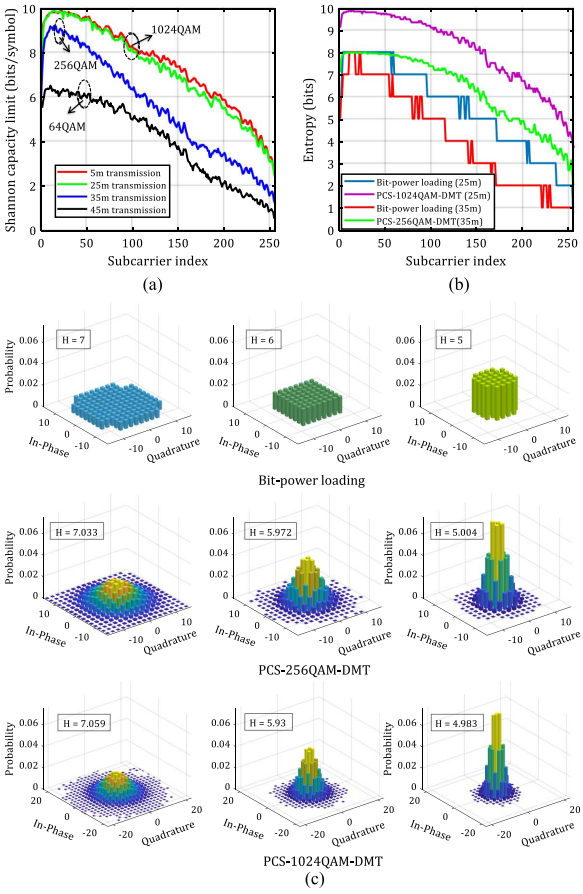

Fig. 4. (a) Shannon capacity limit under different underwater transmission distances. (b) Entropy of different subcarriers for 25 m and 35 m underwater transmission distances. (c) Graphical illustrations for bit-power loading and the PCS-256/1024QAM-DMT scheme of three different entropies. Note that the bars denote the probability of each modulation symbol[42].

points may tend to zero for stronger shaping resulting from the PCS-QAM.

Figures 5(a)–5(c) depict the corresponding received constellation diagrams for bit-power loading, PCS-256QAM-DMT over 35 m, and PCS-1024QAM-DMT over 25 m

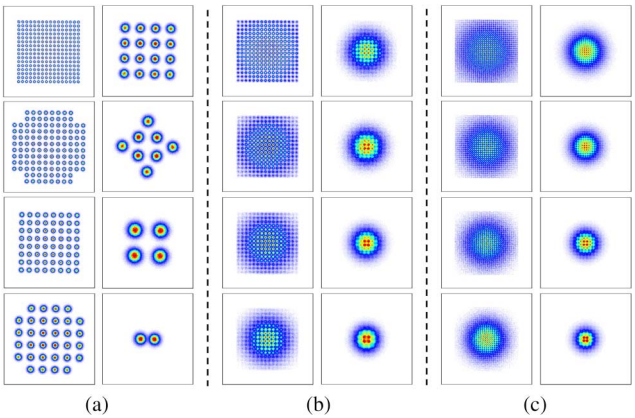

Fig. 5. Received constellation diagrams of (a) bit-power loading, (b) PCS-256QAM-DMT for 35 m, and (c) PCS-1024QAM-DMT for 25 m underwater transmissions[36].

underwater channels, respectively. One can see clearly from Fig. 5 that the constellation points of the bit-power loading scheme are distributed quite uniformly, while the constellation points of PCS-QAM resemble Gaussian distribution. With the PCS-DMT scheme, net data rates of 18.09 Gb/s, 17.21 Gb/s, and 12.64 Gb/s could be achieved after 5 m, 25 m, and 35 m underwater transmission with a modulation bandwidth of ~2.75 GHz, which indicates 32.22%, 30.03%, and 27.55% capacity improvement compared with the widely used bit-power loading DMT scheme in the current UWOC systems[39,40], respectively. More details of the generation, encoding, and decoding of the PCS scheme can be found in Ref. [42].

In this paper, recent research progress has been reviewed for both LED- and LD-based UWOC systems, mainly from a perspective of advanced modulation formats. UWOC systems are susceptible to nonlinearity induced by the components (e.g., LED, LD), which may yield severe impairments in the received signals. Volterra series-based nonlinear equalizers can effectively combat such nonlinear impairments, enhancing the system performance. We have proposed a simplified Volterra nonlinear equalizer by which the SNR received by the system can be enhanced by 2–3 dB. The robustness of the nonlinear equalizer in UWOC systems has also been validated. To further increase the system capacity, the PCS technique has been introduced to address the inherent gap between the conventional regular QAM format and the Shannon capacity of the UWOC system. Together with DMT, a fixed QAM format with different probabilistic distributions has been individually assigned to each subcarrier to achieve the maximum system capacity. Our experimental results have shown a net data rate of 18.09 Gb/s over a 5 m underwater channel, which is the highest data rate ever reported for a single LD in UWOC[42].

This work was supported in part by the National Key Research and Development Program of China (No. 2018YFC1407500), National Natural Science Foundation of China (NSFC) (No. 11621101), and the funding of Ningbo Research Institute.

†The authors contributed equally to this work.

References

1. Oceania, GPM 3000 Acoustic Modem Features, http://www2.l3com.com/oceania//pdfs/datasheets/GPM%20300%20Acoustic%20Modem%20Spec%20Sheet%20Rev%201%206.pdf.
2. I. F. Akyildiz, D. Pompili, and T. Melodia, Ad Hoc Netw. **3**, 257 (2005).
3. Z. Zeng, S. Fu, H. Zhang, Y. Dong, and J. Cheng, IEEE Commun. Surv. Tut. **19**, 204 (2016).
4. H. Kaushal and G. Kaddoum, IEEE Access Underwater Opt. Wireless Commun. **4**, 1518 (2016).
5. N. Saeed, A. Celik, T. Y. Al-Naffouri, and M.-S. Alouini, Ad Hoc Netw. **94**, 101935 (2019).
6. S. Q. Duntley, J. Opt. Soc. Am. **53**, 214 (1963).
7. G. D. Gilbert, T. R. Stoner, and J. L. Jernigan, Proc. SPIE **7**, 3 (1966).
8. Sonardyne International Ltd. http://www.sonardyne.com/products/all-products/instruments/1148-bluecomm-underwater-optical modem.html.
9. R. X. G. Ferreira, E. Xie, J. J. D. McKendry, S. Rajbhandari, H. Chun, G. Faulkner, S. Watson, A. E. Kelly, E. Gu, R. V. Penty, I. H. White, D. C. O'Brien, and M. D. Dawson, IEEE Photon. Technol. Lett. **28**, 2023 (2016).
10. P. Tian, X. Liu, S. Yi, Y. Huang, S. Zhang, X. Zhou, L. Hu, L. Zheng, and R. Liu, Opt. Express **25**, 1193 (2017).
11. H. Lan, I. Tseng, H. Kao, Y. Lin, G. Lin, and C. Wu, IEEE J. Quantum Electron. **54**, 3300106 (2018).
12. S. Watson, M. Tan, S. P. Najda, P. Perlin, M. Leszczynski, G. Targowski, S. Grzanka, and A. E. Kelly, Opt. Lett. **38**, 3792 (2013).
13. C. Lee, C. Zhang, M. Cantore, R. M. Farrell, S. H. Oh, T. Margalith, J. S. Speck, S. Nakamura, J. E. Bowers, and S. P. DenBaars, Opt. Express **23**, 16232 (2015).
14. C. Li, H. Lu, W. Tsai, Z. Wang, C. Hung, C. Su, and Y. Lu, IEEE Photon. J. **10**, 7904909 (2018).
15. A. S. Fletcher, S. A. Hamilton, and J. D. Moores, IEEE Commun. Mag. **53**, 49 (2015).
16. S. Arnon, Opt. Eng. **49**, 015001 (2010).
17. H. Kaushal and G. Kaddoum, IEEE Access Underwater Opt. Wireless Commun. **4**, 1518 (2016).
18. Z. Zeng, S. Fu, H. Zhang, Y. Dong, and J. Cheng, IEEE Commun. Surv. Tut. **19**, 204 (2016).
19. N. Saeed, A. Celik, T. Y. Al-Naffouri, and M.-S. Alouini, Ad Hoc Net. **94**, 101935 (2019).
20. N. Chi and M. Shi, Chin. Opt. Lett. **16**, 120603 (2018).
21. C. Shen, O. Alkhazragi, X. Sun, Y. Guo, T. K. Ng, and B. S. Ooi, Proc. SPIE **10939**, 109390E (2019).
22. L. Wang, S. L. Jacques, and L. Zheng, Comput. Methods Programs Biomed. **47**, 131 (1995).
23. R. M. Lerner and J. D. Summers, Appl. Opt. **21**, 861 (1982).
24. C. Wang, H.-Y. Yu, and Y.-J. Zhu, IEEE Photon. J. **8**, 7906311 (2016).
25. C. Gabriel, M.-A. Khalighi, S. Bourennane, P. Leon, and V. Rigaud, IEEE/OSA J. Opt. Commun. Netw. **5**, 1 (2013).
26. H. Zhang and Y. Dong, IEEE Trans. Wireless Commun. **15**, 1162 (2016).
27. S. Tang, Y. Dong, and X. Zhang, IEEE Trans. Commun. **62**, 226 (2014).
28. H. Zhang and Y. Dong, IEEE Commun. Mag. **54**, 56 (2016).
29. F. Hanson and S. Radic, Appl. Opt. **47**, 277 (2008).
30. J. Xu, M. Kong, A. Lin, Y. Song, X. Yu, F. Qu, J. Han, and N. Deng, Opt. Commun. **369**, 100 (2016).
31. M. Kong, Y. Chen, R. Sarwar, B. Sun, Z. Xu, J. Han, J. Chen, H. Qin, and J. Xu, Opt. Express **26**, 3087 (2018).
32. J. Wang, X. Yang, W. Lv, C. Yu, J. Wu, M. Zhao, F. Qu, Z. Xu, J. Han, and J. Xu, Opt. Commun. **451**, 181 (2019).
33. F. Wang, Y. Liu, F. Jiang, and N. Chi, Opt. Commun. **425**, 106 (2018).
34. N. Chi, Y. Zhao, M. Shi, P. Zou, and X. Lu, Opt. Express **26**, 26700 (2018).
35. H. M. Oubei, J. R. Duran, B. Janjua, H. Y. Wang, C. T. Tsai, Y. C. Chi, T. K. Ng, H. C. Kuo, J. H. He, M. S. Alouini, G. R. Lin, and B. S. Ooi, Opt. Express **23**, 23302 (2015).
36. Y. Chen, M. Kong, T. Ali, J. Wang, R. Sarwar, J. Han, C. Guo, B. Sun, N. Deng, and J. Xu, Opt. Express **25**, 14760 (2017).
37. C. Y. Li, H. H. Lu, W. S. Tsai, M. T. Cheng, C. M. Ho, Y. C. Wang, Z. Y. Yang, and D. Y. Chen, Opt. Express **25**, 11598 (2017).
38. Y. Huang, C. Tsai, Y. Chi, D. Huang, and G. Lin, IEEE J. Lightwave Technol. **36**, 1739 (2018).

39. C. Fei, J. Zhang, G. Zhang, Y. Wu, X. Hong, and S. He, IEEE J. Lightwave Technol. **36**, 728 (2018).
40. C. Fei, X. Hong, G. Zhang, J. Du, Y. Gong, J. Evans, and S. He, Opt. Express **26**, 34060 (2018).
41. C. Fei, X. Hong, G. Zhang, J. Du, Y. Wang, and S. He, IEEE Photon. Technol. Lett. **31**, 1315 (2019).
42. X. Hong, C. Fei, G. Zhang, J. Du, and S. He, Opt. Lett. **44**, 558 (2019).
43. S. Hu, L. Mi, T. Zhou, and W. Chen, Opt. Express **26**, 21685 (2018).
44. J. Wang, C. Lu, S. Li, and Z. Xu, Opt. Express **27**, 12171 (2019).
45. A. Al-Halafi, H. M. Oubei, B. S. Ooi, and B. Shihada, IEEE/OSA J. Opt. Commun. Net. **9,** 826 (2017).
46. A. Al-Halafi and B. Shihada, IEEE Photon. J. **101**, 7902914 (2018).
47. N. Farr, A. D. Chave, L. Freitag, J. Preisig, S. N. White, D. Yoerger, and F. Sonnichsen, in *OCEANS 2006* (2006).
48. C. Pontbriand, N. Farr, J. Ware, J. Preisig, and H. Popenoe, in *OCEANS 2008* (2008).
49. C. Pontbriand, N. Farr, J. Hansen, J. C. Kinsey, L. P. Pelletier, J. Ware, and D. Fourie, in *OCEANS 2015* (2015).
50. M. Doniec, I. Vasilescu, M. Chitre, C. Detweiler, M. Hoffmann-Kuhnt, and D. Rus, in *OCEANS 2009* (2009).
51. D. Marek and D. Rus, in *IEEE International Conference on Communication Systems* (2010), p. 390.
52. T. Sawa, http://www.godac.jamstec.go.jp/catalog/data/doc_catalog/media/KR17-11_leg2_all.pdf (2017).
53. SUNRISE, http://fp7-sunrise.eu/ (2017).
54. G. Cossu, A. Sturniolo, A. Messa, D. Scaradozzi, and E. Ciaramella, IEEE J. Sel. Areas Commun. **36**, 194 (2018).
55. G. Cossu, A. Sturniolo, A. Messa, S. Grechi, D. Costa, A. Bartolini, D. Scaradozzi, A. Caiti, and E. Ciaramella, J. Lightwave Tech. **36**, 5371 (2018).
56. G. Baiden, Y. Bissiri, and A. Masoti, Ocean Eng. **36**, 633 (2009).
57. G. Baiden and Y. Bissiri, in *OCEANS 2007* (2007).
58. B. Han, W. Zhao, Y. Zheng, J. Meng, T. Wang, Y. Han, W. Wang, Y. Su, T. Duan, and X. Xie, Opt. Commun. **434**, 184 (2019).
59. P. Wang, C. Li, and Z. Xu, IEEE J. Lightwave Technol. **36**, 2627 (2018).
60. X. Shan, C. Yang, Y. Chen, and Q. Xia, in *OCEANS 2017* (2017).
61. J. Baghdady, K. Miller, K. Morgan, M. Byrd, S. Osler, R. Ragusa, W. Li, B. M. Cochenour, and E. G. Johnson, Opt. Express **24**, 9794 (2016).
62. Y. Ren, L. Li, Z. Wang, S. M. Kamali, E. Arbabi, A. Arbabi, Z. Zhao, G. Xie, Y. Cao, N. Ahmed, and Y. Yan, Sci. Rep. **6**, 33306 (2016).
63. A. E. Willner, Z. Zhao, Y. Ren, L. Li, G. Xie, H. Song, C. Liu, R. Zhang, C. Bao, and K. Pang, Opt. Commun. **408**, 21 (2018).
64. Y. Zhao, A. Wang, L. Zhu, W. Lv, J. Xu, S. Li, and J. Wang, Opt. Lett. **42**, 4699 (2017).
65. W. Wang, P. Wang, T. Cao, H. Tian, Y. Zhang, and L. Guo, IEEE Photon. J. **9**, 7905315 (2017).
66. A. Wang, L. Zhu, Y. Zhao, S. Li, W. Lv, J. Xu, and J. Wang, Opt. Express **26**, 8669 (2018).
67. J. Xu, B. Sun, W. Lyu, M. Kong, R. Sarwar, J. Han, W. Zhang, and N. Deng, Opt. Commun. **402**, 260 (2017).
68. X. Sun, W. Cai, O. Alkhazragi, E. N. Ooi, H. He, A. Chaaban, C. Shen, H. M. Oubei, M. Z. M. Khan, T. K. Ng, and M. S. Alouini, Opt. Express **26**, 12870 (2018).
69. X. Sun, M. Kong, C. Shen, C. Kang, T. K. Ng, and B. S. Ooi, Opt. Express **27**, 19635 (2019).
70. H. M. Oubei, E. Zedini, R. T. ElAfandy, A. Kammoun, M. Abdallah, T. K. Ng, M. Hamdi, M.-S. Alouini, and B. S. Ooi, Opt. Lett. **42**, 2455 (2017).
71. Z. Vali, A. Gholami, Z. Ghassemlooy, M. Omoomi, and D. G. Michelson, Appl. Opt. **57**, 8314 (2018).
72. Y. Zhou, X. Zhu, F. Hu, J. Shi, F. Wang, P. Zou, J. Liu, F. Jiang, and N. Chi, Photon. Res. **7**, 1019 (2019).
73. X. Liu, S. Yi, X. Zhou, Z. Fang, Z. J. Qiu, L. Hu, C. Cong, L. Zheng, R. Liu, and P. Tian, Opt. Express **25**, 27937 (2017).
74. K. Ying, Z. Yu, R. J. Baxley, H. Qian, G. K. Chang, and G. T. Zhou, IEEE Wireless Commun. **22**, 36 (2015).
75. T. K. Biswas and W. F. McGee, IEEE Photon. Technol. Lett. **3**, 706 (1991).
76. J. C. Froidure, C. Lebrun, P. Megret, E. Jaunart, P. Goerg, T. Tasia, M. Lamquin, and M. Blondel, IEEE Photon. Technol. Lett. **7**, 266 (1995).
77. J. Kim and K. Konstantinou, Electron. Lett. **37**, 1417 (2001).
78. L. Ding, G. Zhou, D. R. Morgan, Z. Ma, J. S. Kenney, J. Kim, and C. R. Giardina, IEEE Trans. Commun. **52**, 159 (2004).
79. C. Ju, N. Liu, X. Chen, and Z. Zhang, J. Lightwave Technol. **33**, 4997 (2015).
80. G. Stepniak, J. Siuzdak, and P. Zwierko, IEEE Photon. Technol. Lett. **25**, 1597 (2013).
81. Y. Wang, L. Tao, X. Huang, J. Shi, and N. Chi, IEEE Photonics J. **7**, 7901907 (2015).
82. C. Eun and E. J. Powers, IEEE Trans. Signal Process. **45**, 223 (1997).
83. F. P. Guiomar, J. D. Reis, A. L. Teixeira, and A. N. Pinto, Opt. Express **20**, 1360 (2012).
84. G. Zhang, J. Zhang, X. Hong, and S. He, Opt. Express **25**, 3780 (2017).
85. G. Zhang, C. Fei, S. He, and X. Hong, in *Asia Communications and Photonics Conference (ACP)* (2017), paper Su2A.75.
86. G. Zhang, X. Hong, C. Fei, and X. Hong, J. Lightwave Technol., early access (2019).
87. J. W. Giles and I. N. Bankman, in *Proceedings of IEEE Military Communication Conference* (2005), p. 1700.
88. G. Böcherer, F. Steiner, and P. Schulte, IEEE Trans. Commun. **63**, 4651 (2015).
89. F. Buchali, F. Steiner, G. Böcherer, L. Schmalen, P. Schulte, and W. Idler, J. Lightwave Technol. **34**, 1599 (2016).
90. T. Fehenberger, A. Alvarado, G. Böcherer, and N. Hanik, J. Lightwave Technol. **34**, 5063 (2016).
91. C. Xie, Z. Chen, S. Fu, W. Liu, Z. He, L. Deng, M. Tang, and D. Liu, Opt. Express **26**, 367 (2018).
92. T. M. Cover and J. A. Thomas, *Elements of Information Theory*. (John Wiley & Sons, 2006).